Int. J. Heat Mass Transfer. Vol. 31, No. 6, pp. 1177–1187, 1988
Printed in Great Britain

0017-9310/88 $3.00 + 0.00

Laminar natural convection heat transfer from sharp-edged horizontal bars with flow separation

K. S. CHANG, C. J. CHOI† and C. H. CHO

Department of Mechanical Engineering, Korea Advanced Institute of Science and Technology, P.O. Box 150, Cheongryang, Seoul, Republic of Korea

(*Received* 26 *June* 1987 *and in final form* 28 *October* 1987)

Abstract—Laminar natural convection over a sharp-edged horizontal bar situated in an infinite fluid medium has been investigated numerically and experimentally. Finite-difference solutions to the two-dimensional Navier–Stokes and energy equations were obtained with a fixed Prandtl number of 0.7 for the two configurations: a flat plate of finite thickness and a square bar. The difficulty associated with the complex physical flow domain was overcome by using the body-fitted coordinates. In the numerical study we found no indication of flow separation for the flat plate, in the range of Rayleigh number $10^3 \leqslant Ra \leqslant 10^5$. For the square bar, however, the boundary layer separated easily at the upper sharp edges for $Ra \geqslant 5 \times 10^3$ and well-defined twin vortices were identified above the upper horizontal surface. A Mach–Zehnder interferometric study was concurrently carried out in air for the square bar to determine the local temperature and Nusselt number distributions in the Rayleigh number range $1.95 \times 10^4 \leqslant Ra \leqslant 1.53 \times 10^5$. Comparison of the two results, the numerical and the experimental, offered good agreement.

INTRODUCTION

LAMINAR natural convection about heated bodies has been investigated extensively. Most of the earlier studies are, in general, limited to natural convection without flow separation. The flow separated from a bluff body is of inherent interest in fluid mechanics since the wall heat flux or the wall pressure can be significantly influenced by its existence. In forced convection, flow separation is attributed to the reaction of the viscous boundary layer to a pressure field established in an adjacent outer inviscid flow region. In contrast, the flow separation mechanism in the natural convection is complicated because the buoyancy force which is not necessarily aligned with the body surface operates as a body force in the entire boundary layer.

Flow separation in natural convection seems to have been very elusive and did not receive due attention in the literature. Bromhan and Mayhew [1] reported from smoke tests the observation of a small separated flow region at the base of a plume rising from a heated sphere. Schenk and Schenkels [2] carried out an experimental study with an ice sphere melting in water. They observed that the downward boundary layer, generated by a prevailing positive thermal expansion coefficient above 4°C, separates ahead of the bottom stagnation point.

For two-dimensional natural convection, Pera and Gebhart [3] concluded by experimental observation of the wake formation over a circular cylinder in water that the flow separation did not exist in the natural convective flow adjacent to the smooth body surface. Another experimental study includes one for a horizontal semi-infinite flat plate: the interferometry performed by Rottem and Claassen [4], semi-focusing colour Schlieren photography, revealed that the boundary layer on the upper surface of the plate broke down into a large eddy instability at some distance from the leading edge. Pera and Gebhart [5, 6] and Gebhart [7, 8] also confirmed by smoke visualization the existence of such a laminar boundary layer near the leading edge above a heated horizontal surface.

The possibility of flow separation in the natural convective flow about a heated square bar was first reported in ref. [9]. From the peculiar temperature inversion phenomenon, first fortuitously found in the Mach–Zehnder interferograms in the Grashof number range 2.77×10^4–2.19×10^5, the existence of twin vortices above the upper horizontal surface of the square bar was conjectured. In an earlier related paper [10], however, where the finite element method and the smoke visualization of the streamlines were used to study the natural convection between a concentric square bar and an outer horizontal circular cylinder, this phenomenon was absent due to the relatively low Rayleigh number range of investigation, $Ra < 10^5$. For the same problem with Rayleigh numbers greater than 10^6, Cho [11] suggested with experimental evidence that flow separates at the sharp upper edges of the square bar. Recently, Miyamoto *et al.* [12] reported on the heat transfer from rectangular prisms, the aspect ratio of which is varied from a vertical plate to a horizontal one. Their analysis using the finite difference method, which is limited to a relatively low Rayleigh number 1.94×10^4, suggested the existence of a separated bubble above the upper surface of the

† Present address: Korea Advanced Energy Research Institute, P.O. Box 7, Dae-Duk, Choong-Nam, Republic of Korea.

NOMENCLATURE

g	gravitational acceleration
Gr	Grashof number, $g\bar{\beta}L^3(T_w-T_0)/\nu^2$
h	local heat transfer coefficient
k	thermal conductivity
L	side length of a square bar or length of a flat plate
L	operator, $L^lF=[(f_\xi F)_\eta-(f_\eta F)_\xi]/J$
M	operator, $Mf=\gamma f_\eta-\beta f_\xi$ on $\eta=$ const.; $Mf=\alpha f_\xi-\beta f_\eta$ on $\xi=$ const.
n	coordinate in the normal direction
Nu	local Nusselt number, hL/k
P,Q	coordinate control functions
Pr	Prandtl number, $\nu/\bar{\alpha}$
Ra	Rayleigh number, $g\bar{\beta}L^3(T_w-T_0)/\nu\bar{\alpha}$
t	dimensionless time, $\bar{t}/(L^2/\bar{\alpha})$
T	temperature
u,v	velocity components along x,y direction, $(\bar{u},\bar{v})/(\bar{\alpha}/L)$
x,y	dimensionless Cartesian coordinates, $(\bar{x},\bar{y})/L$.

Greek symbols

$\bar{\alpha}$	thermal diffusivity
$\bar{\beta}$	thermal expansion coefficient
ε	convergence criterion
ζ	dimensionless vorticity, $\bar{\zeta}/(\bar{\alpha}/L^2)$
θ	angle
ν	kinematic viscosity
ξ,η	coordinates in the transformed plane
ρ	demarcation angle for the outflow boundary conditions
ϕ	dimensionless temperature, $(T-T_0)/(T_w-T_0)$
ψ	dimensionless stream function, $\bar{\psi}/\bar{\alpha}$.

Subscripts

0	reference value
w	wall surface.

Superscript

¯	dimensional quantities.

rectangular bar. More recently, Chang and Choi [13] presented a brief account of the flow separation from the upper edges of a hot square bar through a numerical analysis.

In this paper, two flow models were chosen: a horizontal flat plate of finite thickness and a horizontal square bar, both isothermal and infinitely long. The former can be regarded as an extreme case of a rectangular bar, where we took for convenience the aspect ratio of the cross-section (the thickness divided by the width) as 0.01. Although the flow geometries look unusual, they have practical industrial applications in the cooling of integrated circuit chips and other components. The study also has fundamental importance in understanding how a buoyant boundary layer separates past sharp edges and how the heat transfer characteristics are accordingly affected.

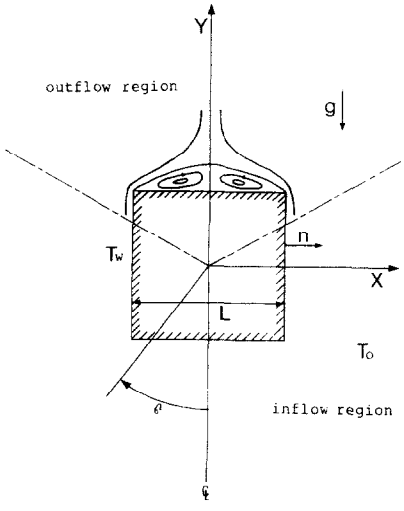

FIG. 1. Schematic diagram of the flow over a square bar.

NUMERICAL STUDY

Mathematical formulation

One of the two physical models is pictured schematically in Fig. 1. A horizontal square bar of dimension $L\times L$ is situated in an infinite air medium of temperature T_0. The bar is kept at a higher uniform temperature T_w. Symmetry with respect to the vertical mid-plane is assumed. If the symmetry cannot be assured for some reason, a full flow domain should be taken into account rather than half. In the present study, this symmetry has been carefully monitored through Mach–Zehnder interferometry. The broken line in Fig. 1 represents the demarcation line across which the inflow and the outflow boundary conditions are differentiated on the far boundary.

We used the Boussinesq approximation for two-dimensional steady laminar natural convective flow. The non-dimensional form of the governing equations is, in Cartesian coordinates

$$\zeta_t+u\zeta_x+v\zeta_y=Pr\nabla^2\zeta+Ra\,Pr\,\phi_x \tag{1}$$

$$\zeta=-\nabla^2\psi \tag{2}$$

$$\phi_t+u\phi_y+v\phi_y=\nabla^2\phi \tag{3}$$

where

$$u=\psi_y,\quad v=-\psi_x.$$

Ellipticity of the above governing differential equations demands boundary conditions on the entire boundary enclosing the flow field, while their parabolicity requires the description of the initial condition. The inner boundaries are made of the body wall and the lines of symmetry where we specify

$$\psi = 0, \quad \zeta = -\psi_{nn}, \quad \phi = 1 \qquad \text{on the wall}$$
$$\psi = \zeta = \phi_n = 0 \qquad \text{on the line of symmetry.} \quad (4)$$

Natural convection about a horizontal circular cylinder in an infinite fluid medium was previously calculated by Kuehn and Goldstein [14], and Farouk and Guceri [15]. They justifiably thought that on the far boundary the fluid either enters or leaves the domain radially; on the outflow boundary, the temperature of the leaving fluid satisfies a Neumann condition. Then, on the inflow boundary

$$\psi_n = \zeta_n = \phi = 0 \quad \text{where } 0 \leqslant \theta < \rho \qquad (5)$$

and on the outflow boundary

$$\psi_n = \zeta_n = \phi_n = 0 \quad \text{where } \rho \leqslant \theta \leqslant \pi. \qquad (6)$$

For good accuracy, the pseudo far boundary of the finite computational domain should be located as far from the body as possible. Through extensive test calculations, we found that the circular pseudo far boundary located at a distance $8L$ or more from the centre of the body is sufficient, causing virtually no change to the solution near the body.

The demarcation between the inflow and the outflow on the pseudo far boundary can be determined by observing the interferograms. The outflow boundary should be chosen large enough to cover the buoyant thermal plume region. It is found that the numerical solution is rather insensitive to the change of the demarcation as long as the rising plume is properly treated by the outflow condition. We fixed the demarcation at $\rho = 0.7\pi$ for all the calculations made in the present paper.

Method of solution

It is important that the coordinate system conforms to the boundary shape of the flow region. In this paper, mapping of the flow domain (Fig. 2) is carried out by a general clustered curvilinear coordinate system, patterned after Steger and Sorenson [16]. Application of this kind of general body-fitted coordinate has not been frequently made in the heat transfer area. One exception is a melting problem considered by Rieger *et al.* [17, 18].

The boundary-fitted coordinate system is generated numerically by solving a system of elliptic equations

$$\tilde{\nabla}^2 x = 0, \quad \tilde{\nabla}^2 y = 0 \qquad (7)$$

with Dirichlet boundary conditions. The transformed Laplace operator contains coordinate control functions P and Q, which can influence the structure of the grid if properly chosen

$$\tilde{\nabla}^2 \equiv \{\alpha\partial_{\xi\xi} - 2\beta\partial_{\xi\eta} + \gamma\partial_{\eta\eta} + J^2(P\partial_\xi + Q\partial_\eta)\}/J^2 \qquad (8)$$

where

$$\alpha = x_\eta^2 + y_\eta^2, \qquad \gamma = x_\xi^2 + y_\xi^2$$
$$\beta = x_\xi x_\eta + y_\xi y_\eta, \quad J = x_\xi y_\eta - x_\eta y_\xi.$$

It is known that the accuracy of computation is improved in association with applying the boundary conditions, if near-orthogonality of the coordinates is maintained around the boundary in the general coordinate system. Here, the source terms P and Q were determined by enforcing the orthogonality condition at the boundary points and by assigning the minimum grid distance from the body. For more information see ref. [16].

The given set of governing equations (1)–(3) as well as the boundary conditions are accordingly transformed. It is noted that the unsteady terms included in the present formulation permit the powerful alternating direction implicit (ADI) computation, later. The results are

$$\zeta_t + L^\psi \zeta = Pr\,\tilde{\nabla}^2\zeta + Ra\,Pr\,L^y\phi \qquad (9)$$
$$\tilde{\nabla}^2\psi = -\zeta \qquad (10)$$
$$\phi_t + L^\psi\phi = \tilde{\nabla}^2\phi. \qquad (11)$$

The boundary conditions are transformed as follows:

$$\psi = \zeta = 0, \quad M\phi = 0 \qquad \text{on the symmetry line}$$
$$\psi = 0, \quad \zeta = -\frac{\bar{\gamma}\psi_{\eta\eta}}{J^2}, \quad \phi = 1 \qquad \text{on the wall}$$
$$M\psi = M\zeta = \phi = 0 \qquad \text{on the inflow region}$$
$$M\psi = M\zeta = M\phi = 0 \qquad \text{on the outflow region.} \quad (12)$$

The transformed vorticity transport equation and the energy equation are solved by the ADI technique. For the stream function equation the successive over-relaxation (SOR) method is appropriate. All the derivatives with respect to and including the convection terms, are approximated by the central difference schemes. Convergence was achieved with the criterion $|B^{n+1} - B^n|/|B^{n+1}| < \varepsilon$. The value of ε taken for the convergence was 0.001 for both the vorticity ($B = \varepsilon$) and the temperature, and 0.01 for the stream function.

Results

Numerical solutions are obtained for the two sharp-edged models so that the effect of geometry on the flow separation can be identified. The Prandtl number is fixed at 0.7 throughout the numerical study, while the Rayleigh number is changed to several selected values in the laminar convection regime.

The grid systems used for calculation are shown near the body in Fig. 3. The grid distance is made smallest near the heated surface and is gradually expanded in the outer region. For a flat plate and a

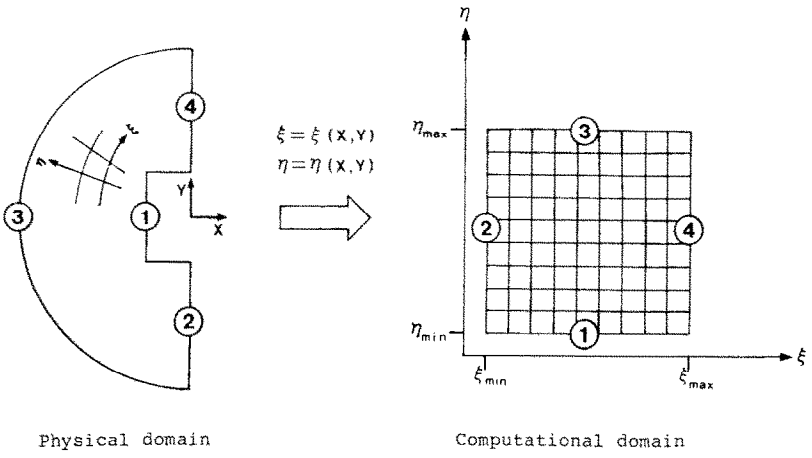

FIG. 2. Coordinates transformation.

square bar in the computational domain (ξ, η) 51×81 and 54×81 grid points were used, respectively.

Figure 4 shows representative temperature and stream function contours for a flat plate at $Ra = 5 \times 10^4$. Flow patterns remain very similar for various Rayleigh numbers from 10^3 to 10^5. The isotherms are dense near the surface and formation of the thermal boundary layer and the buoyant plume is evident, convecting heat away from the body.

The flow did not separate during the 180°-turn around the sharp edges. The self-closed streamlines in the flow field, which are indisputable evidence of a separated flow, were not computed above the upper surface in Fig. 4. In contrast, Miyamoto *et al.*'s calculation [12] showed a small separation bubble on the upper surface of a horizontal plate near the sharp edges at $Ra = 6.48 \times 10^3$ and for $Pr = 0.72$. They suggested that this separation bubble caused instability and induced flow asymmetry above the flat plate. In our numerical calculation, however, the separation bubble which had appeared during the time marching process finally vanished as the solution converged to the steady state.

Distribution of the local Nusselt number scaled by $Ra^{1/4}$ is plotted for the flat plate in Fig. 5 for three different Rayleigh numbers. The heat transfer coefficient has a peak near the sharp edge and its value at the centre of the plate is greater on the lower surface than on the upper one. Experimental study of a flat plate heated on the downward-facing surface was performed by Aihara *et al.* [19]. Restrepo and Glicksman [20] experimentally studied natural convection from

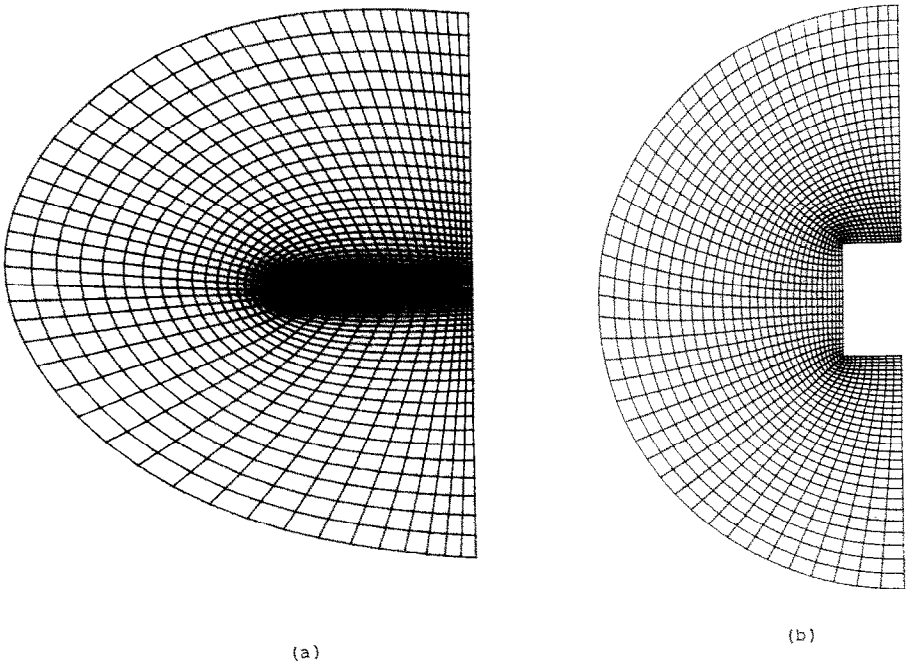

FIG. 3. Grid systems near a flat plate (a) and a square bar (b).

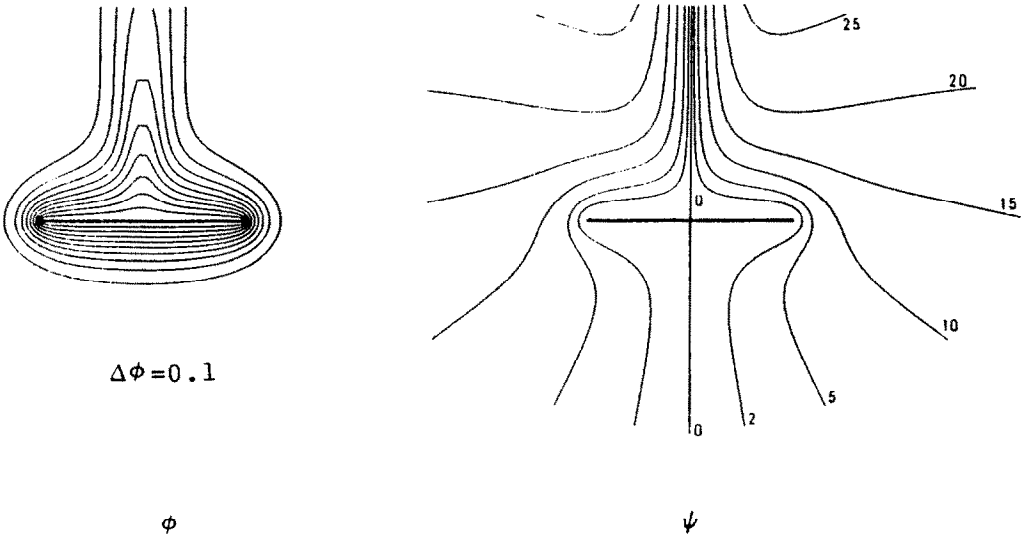

FIG. 4. Isotherms and streamlines for a flat plate ($Ra = 5 \times 10^4$).

a finite horizontal square plate heated again on the downward face in air. These results are also plotted in Fig. 5.

Figures 6(a)–(c) show the contour lines of constant temperature and constant stream function for a square bar at increasing Rayleigh numbers. Because of the alignment of the buoyancy force with the body surface, the convective flow gains more momentum along the vertical surface than along the horizontal one. The isotherms around a horizontal square bar at $Ra = 10^3$ presented in Fig. 6(a) are globally similar to those from a circular cylinder [14]. At higher Rayleigh numbers, the thermal boundary layer around the square bar and the buoyant plume become more distinctive as observed from Figs. 6(b) and (c). As the flow accelerated by the heated vertical surface reaches the end of the surface, it cannot make a sudden turn at the sharp edges where the wall curvature is infinite, resulting in a flow separation. However, in the case of insufficient flow acceleration, separation of flow is not assured at the sharp edges. The less heated flow at $Ra = 10^3$ in Fig. 6(a), the attached boundary layer flows around the lower sharp edges at high Rayleigh numbers in Figs. 6(b) and (c), and the flow around a horizontal flat plate in Fig. 4 are examples. In Fig. 6(b), the separated flow region above the upper surface causes a little dent on the innermost isothermal line. As the Rayleigh number is increased to 1.53×10^5, Fig. 6(c), a characteristic finger print appears in the pattern of isotherms, and the separated flow turns into active twin vortices. The depressed isotherms in the separated flow region resemble an ice-cream scoop, with temperature inversion in the circumferential direction.

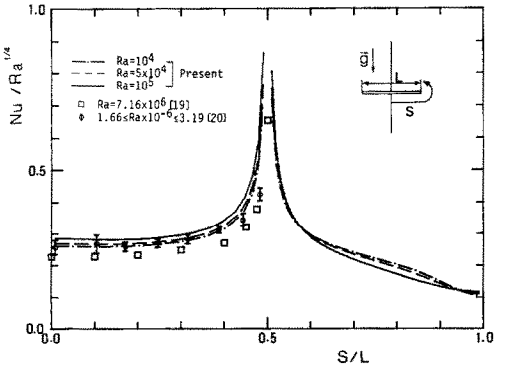

FIG. 5. Local Nusselt number distributions for a flat plate.

Local Nusselt number is plotted in Fig. 7 for a square bar with the Rayleigh number as a parameter. As the Rayleigh number is increased, near-similarity is obtained along the vertical surface. In contrast, this similarity is lost along the horizontal surfaces. Both when the separated flow does not exist and when the strength of the twin vortices generated by the flow separation is weak, the local Nusselt number decreases monotonously with the horizontal distance from the upper sharp edge. However, with strong twin vortices above the cylinder the local Nusselt number has a local peak at the centre of the upper horizontal surface. It is due to the downwash in the region near the symmetry line caused by the counter-rotating twin vortices. Having released its thermal energy by conduction to the external fluid during the vortical motion, the flow in the downwash is at relatively low temperature.

The local Nusselt number distribution along the wall is shown for $Ra = 3.56 \times 10^4$ in Fig. 8. Previous experimental results obtained at $Gr = 5.72 \times 10^4$ in air by Eckert and Soehngen [21] are shown by squares. Miyamoto *et al.*'s numerical result is also plotted [12], although their calculation was done at $Ra = 1.94 \times 10^4$ and $Pr = 0.72$. It is noted that all the results have the same trend qualitatively. Particularly, the present numerical results are observed to be in

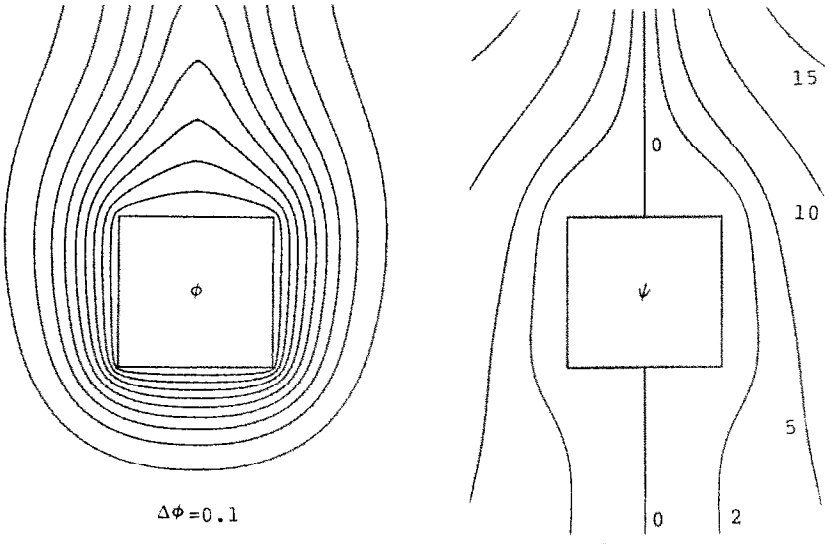

FIG. 6(a). Isotherms and streamlines ($Ra = 10^3$).

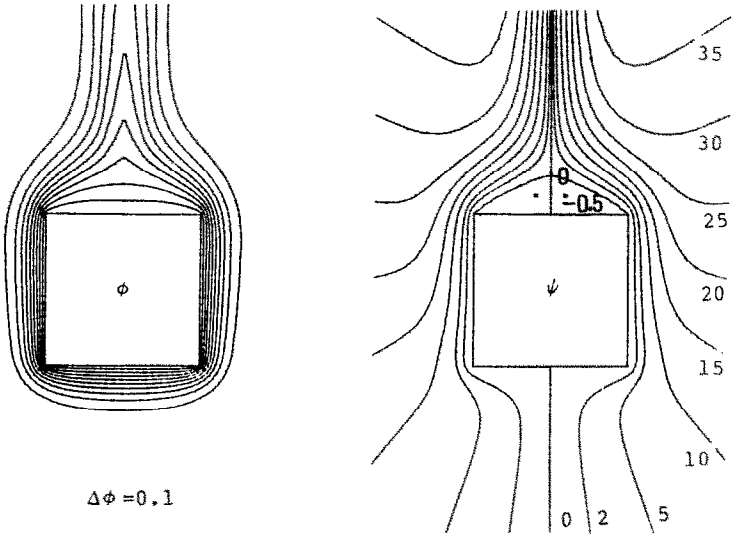

FIG. 6(b). Isotherms and streamlines ($Ra = 3.56 \times 10^4$).

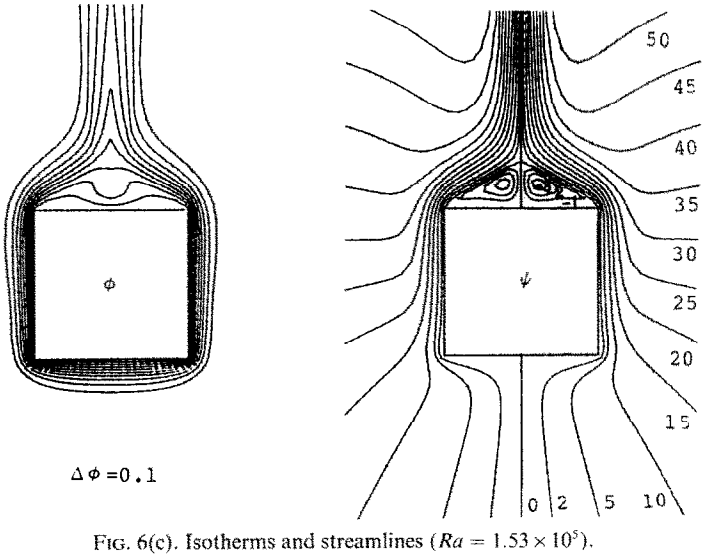

FIG. 6(c). Isotherms and streamlines ($Ra = 1.53 \times 10^5$).

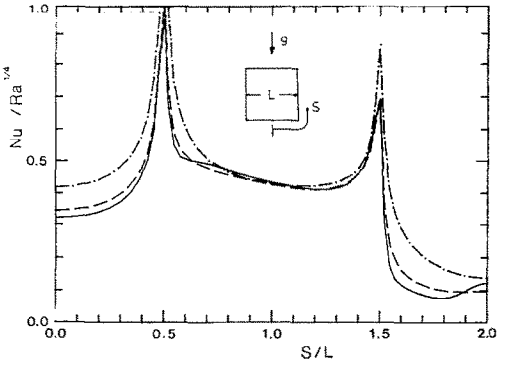

FIG. 7. Local Nusselt number distributions for a square bar: —·—, $Ra = 10^3$; – – –, $Ra = 3.56 \times 10^4$; ——, $Ra = 1.53 \times 10^5$.

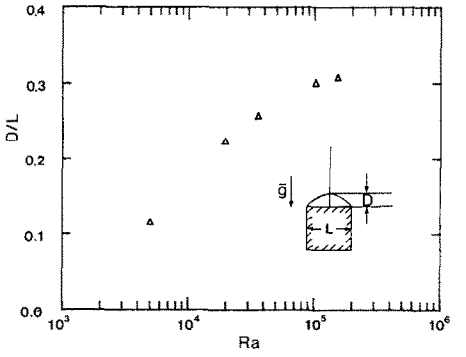

FIG. 9. Height of the closed bubbles.

good agreement with the previous experiment by Eckert and Soehngen [21].

For the flow past a circular cylinder, the flow remains attached to the body for a Reynolds number less than 5. In the Reynolds number range from 5 to 40, the flow pattern allows stationary twin vortices in the separated region behind the cylinder. For a Reynolds number greater than 40, the flow finally becomes unsteady and shedding of the vortices occurs in an alternating form [22]. In contrast, the separated natural convection above a square bar retains stationary twin vortices even for relatively large Rayleigh numbers. The height of the closed streamline region above a square bar is shown in Fig. 9. It is unlikely, however, these twin vortices break in a shedded form without first introducing flow instability and transition to turbulence when the Rayleigh number is further elevated.

EXPERIMENTAL STUDY

Apparatus

A test model shown in Fig. 10, designed to operate in air at atmospheric pressure, was built for a Mach–Zehnder interferometer of 20 cm mirror size. The model was housed in a relatively large acryl chamber, where a pair of quartz windows were installed on the chamber wall for the beam path. A 10 mW He–Ne laser was used as a light source. The assembled apparatus was then sufficiently free from environmental air disturbances.

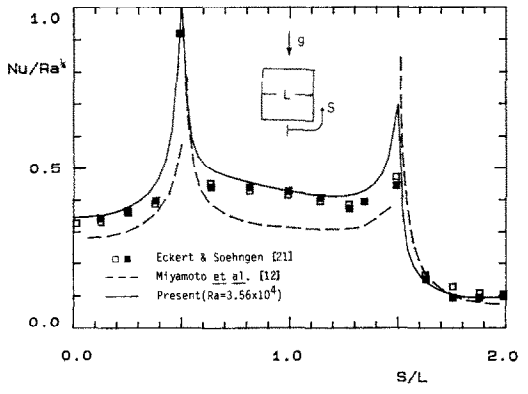

FIG. 8. Local Nusselt number for a square bar.

Two different test models were manufactured from welded square copper pipes by machining their outer surfaces. One square bar had external dimensions of $2.43 \times 2.43 \times 30.10$ cm with a wall thickness of 0.31 cm, and the other had external dimensions of $3.90 \times 3.90 \times 25.02$ cm. The first model was used for relatively low Rayleigh numbers and the second for Rayleigh numbers larger than 1.02×10^5. The cylinder was heated internally by a coiled 20 Ω electrical resistance wire with conductive substances such as iron and magnesium powder packed in the rest of the inner space. End insulators made of polystyrene square plates were installed at the ends of the square bar. In order to attain uniformity of the surface temperature, iron and magnesium powders mixed in different ratios in different azimuthal directions were used. To check longitudinal temperature uniformity, five thermocouples were installed on the upper surface; the circumferential uniformity was monitored by the four thermocouples, installed one on each side at three different cross-sections. An individual thermocouple was calibrated to an accuracy of 0.1°C. The maximum deviation from uniformity was 0.5% in the azimuthal direction and 0.4% in the longitudinal.

In the finite-sized test chamber where thermal stratification may cause an unfavorable effect on the convection, some special treatment was required. Because each fringe number in the interferogram indicated a 3°C temperature increment in the 25 cm optical path, a slight thermal stratification would disturb the fringe pattern noticeably. The problem was overcome by curtailing the transition time until a steady state was reached, by imposing a large heating rate initially. By this procedure the maximum thermal stratification was reduced to 0.007°C cm^{-1} at worst.

Procedure

The operational principle of a Mach–Zehnder interferometer was described by Hauf and Grigull [23]. The input power was supplied by a HP 6255A dual d.c. power supply. All the data were either stored on

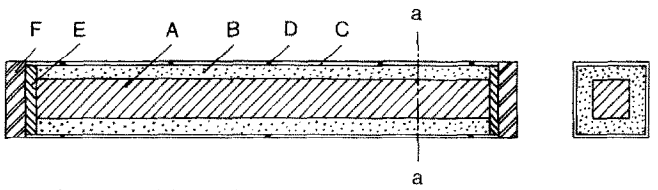

FIG. 10. Experimental test model: A, heater; B, iron and magnesium powders; C, copper pipe; D, thermocouple; E, polystyrene; F, yellow pine wood.

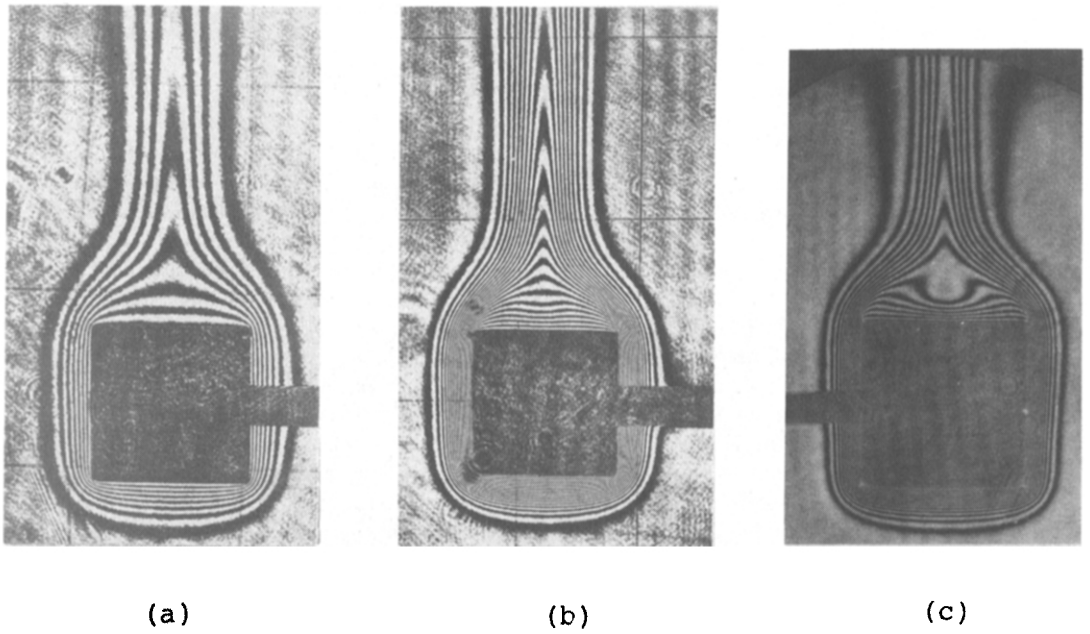

FIG. 11. Interferograms for a square bar: (a) $Ra = 1.95 \times 10^4$, $Pr = 0.704$; (b) $Ra = 3.56 \times 10^4$, $Pr = 0.696$; (c) $Ra = 1.53 \times 10^5$, $Pr = 0.700$.

a cassette tape or printed using a Commodore 2001 series PET micro-computer and a HP 3465A digital multimeter. The analogue signal from the thermocouples, the voltage and the current of the power supply were automatically recorded at every 10 min intervals. All photographs were taken on ASA 100 Neopan SS fine grain panchromatic film using a Nikon F-3 camera. The total running time was about 2–3 h.

The overall heat transfer was determined either from the real input power or from the interferograms. The two had a discrepancy and a compensation was necessary: the thermal radiation loss was approximately determined by using the Stefan–Boltzmann equation. This generally was larger than the estimated two-dimensional heat loss due to the end effect.

Results

The interferograms are presented in Figs. 11(a)–(c) for three different Rayleigh numbers. The fringes can be considered as isotherms since the index of refraction is a function of temperature only in natural convection. The air properties at the mean of the two temperatures T_w and T_0 were used here to evaluate the Rayleigh number, the Prandtl number and the Nusselt number.

In Fig. 11(a) at $Ra = 1.95 \times 10^4$, the largest distance between isotherms or the smallest temperature gradient occur along the upper symmetric line. In natural convection, when there are two or more counter-streamings in a confined area, it is common that the curvature of the isotherms change their sign and the isotherms are bulged in the flow direction, which usually cause the phenomenon of temperature inversion. In Fig. 11(b) at $Ra = 3.56 \times 10^4$, it is observed that even for an external convection the isotherms near the body are slightly depressed toward the wall in the upper symmetry region. The central compression of the isotherms is even more amplified, even to the form of the earlier ice-cream scoop, in Fig. 11(c) for $Ra = 1.53 \times 10^5$. This phenomenon suggests that there is evidently a downwash in the convective stream over the upper horizontal surface near the symmetric line. Recall that it has been shown from the earlier computational results, Fig. 6, that the compression or even the flatness of the isotherms in this region is directly related to the separated flow appearing in the form of counter-rotating twin vortices.

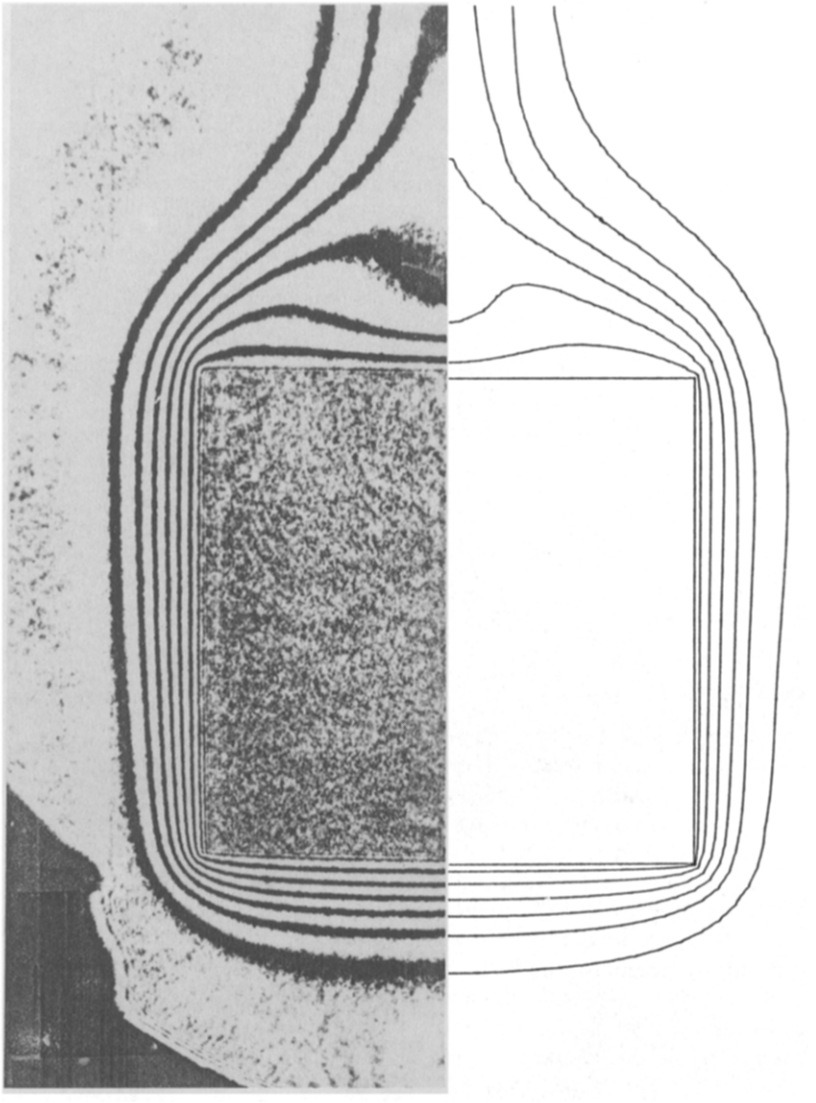

FIG. 12. Comparison of experimental and numerical isotherms.

	Experimental	Numerical
Ra	9.7×10^4	1.02×10^5
Pr	0.709	0.7

In Fig. 12, direct comparison of the isotherms from the present experiment (left) and the computation (right) is presented. The seven isotherms well matched below the bottom of the cylinder do not perfectly coincide above the upper surface. Nevertheless, the overall agreement in the qualitative trend is indisputable. The readers are referred here back to Fig. 8 where the computational local Nusselt number was quantitatively well compared with the heat flux measurement of Eckert and Soehngen [21].

The average heat transfer coefficient obtained from the experiment and the computation is given in Fig. 13. The agreement is reasonable in the range $1.95 \times 10^4 \leqslant Ra \leqslant 10^5$. For a higher Rayleigh number range, however, the large radiational energy loss and the end wall effect could probably be blamed for the deviation of the data. For a Rayleigh number lower than 1.95×10^4, the size of the test model had to be reduced and a reduced temperature scale used. The insufficient number of fringes in the interferogram in this case made the present experimental results very unreliable and the idea of extracting any useful information from the interferometry had to be abandoned. For a two-dimensional square bar, King's correlation [24] can be rewritten as

$$\overline{Nu} = 0.357 Ra^{1/4} \tag{13}$$

by using the side length of the bar as a characteristic

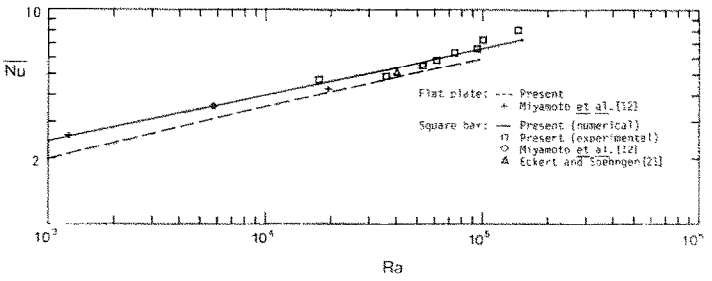

FIG. 13. Average Nusselt number for a flat plate and a square bar.

length. From the experimental data in the present study, the average Nusselt number can be correlated by least-square regression analysis in the range $3\times10^4 < Ra < 2\times10^5$ as

$$\overline{Nu} = 0.856Ra^{0.177}. \quad (14)$$

If one prefers to fit the data in one-fourth power law, the correlation would become

$$\overline{Nu} = 0.376Ra^{1/4}. \quad (15)$$

SUMMARY AND CONCLUSIONS

Solution to the Navier–Stokes and energy equations has been obtained for the natural convection heat transfer from a horizontal, isothermal, sharp-edged object such as a flat plate or a square bar. Some of these convections have also been experimentally studied. The flow pattern around a flat plate shows no flow separation at the sharp edges in the Rayleigh number range considered. Similarly, it has been shown for a square bar that the strong thermohydraulic interference between the adjacent walls causes the thermal boundary layer to follow closely the body configuration with no premature flow separation, if the Rayleigh number is sufficiently low of the order of 10^3. In contrast, it has been disclosed that for higher Rayleigh numbers a separated flow pattern is possible above the upper horizontal surface of a square bar. The temperature inversion in the circumferential direction, which is the consequence of the active twin vortices, is found when the Rayleigh number becomes of the order of 10^5. The separated flow was maintained in a closed bubble form to the highest Rayleigh number calculated, without any indication of bursting. The local and average Nusselt numbers are obtained. It is found that the flow separation causes the local heat transfer to increase on the upper horizontal surface of a square cylinder, but not the overall heat transfer. Comparison between the numerical and the experimental results has demonstrated good agreement overall.

REFERENCES

1. R. J. Bromhan and Y. R. Mayhew, Free convection from a sphere in air, *Int. J. Heat Mass Transfer* **2**, 83–84 (1962).
2. J. Schenk and F. A. A. Schenkels, Thermal free convection from an ice sphere in water, *Appl. Scient. Res.* **19**, 465–476 (1968).
3. L. Pera and B. Gebhart, Experimental observations of wake formation over cylindrical surfaces in natural convection flows, *Int. J. Heat Mass Transfer* **15**, 175–177 (1972).
4. Z. Rottem and L. Claassen, Natural convection above unconfined horizontal surfaces, *J. Fluid Mech.* **39**, 173–192 (1969).
5. L. Pera and B. Gebhart, Natural convection boundary layer flow over horizontal and slightly inclined surfaces, *Int. J. Heat Mass Transfer* **16**, 1131–1146 (1973).
6. L. Pera and B. Gebhart, On the stability of natural convection boundary layer flow over horizontal and slightly inclined surface, *Int. J. Heat Mass Transfer* **16**, 1147–1163 (1973).
7. B. Gebhart, Natural convection flows and stability, *Adv. Heat Transfer* **9**, 173–348 (1973).
8. B. Gebhart, Buoyancy induced fluid motions characteristic of applications in technology—the 1978 Freeman scholar lecture, *Trans. ASME I: J. Fluids Engng* **101**, 5–28 (1979).
9. C. H. Cho and K. S. Chang, Experimental observations of temperature inversions over the horizontal square cylinder in natural convection, *Int. Commun. Heat Mass Transfer* **11**, 275–281 (1984).
10. K. S. Chang, Y. H. Won and C. H. Cho, Patterns of natural convection circular cylinder, *Trans. ASME C: J. Heat Transfer* **105**, 173–180 (1983).
11. C. H. Cho, Laminar natural convection heat transfer about a heated horizontal cylinder having an attached or separated plume, Ph.D. thesis, KAIST (1985).
12. M. Miyamoto, Y. Katoh, J. Kurima, S. Kurihara and K. Yamashita, Free convection heat transfer from vertical and horizontal short plates, *Int. J. Heat Mass Transfer* **28**, 1733–1745 (1985).
13. K. S. Chang and C. J. Choi, Separated laminar natural convection above a horizontal isothermal square cylinder, *Int. Commun. Heat Mass Transfer* **13**, 201–208 (1986).
14. T. H. Kuehn and R. J. Goldstein, Numerical solution to the Navier–Stokes equations for laminar natural convection about a horizontal isothermal circular cylinder, *Int. J. Heat Mass Transfer* **23**, 971–979 (1980).
15. B. Farouk and S. I. Guceri, Natural convection from a horizontal cylinder—laminar regime, *Trans. ASME C: J. Heat Transfer* **103**, 522–527 (1981).
16. J. L. Steger and R. L. Sorenson, Automatic mesh-point clustering near a boundary in grid generation with elliptic partial differential equations, *J. Comput. Phys.* **33**, 405–410 (1979).
17. H. Rieger, U. Projahn and H. Beer, Analysis of the heat transport mechanisms during melting around a horizontal circular cylinder, *Int. J. Heat Mass Transfer* **25**, 137–147 (1982).
18. H. Rieger, U. Projahn, M. Bareiss and H. Beer, Heat transfer during melting inside a horizontal tube, *Trans. ASME C: J. Heat Transfer* **105**, 226–234 (1983).

19. T. Aihara, Y. Yamada and S. Endo, Free convection along the downward-facing surface of a heated horizontal plate, *Int. J. Heat Mass Transfer* **15**, 2535–2549 (1972).
20. F. Restrepo and L. R. Glicksman, The effect of edge conditions on natural convection from a horizontal plate, *Int. J. Heat Mass Transfer* **17**, 135–142 (1974).
21. E. R. G. Eckert and E. E. Soehngen, Studies on heat transfer in laminar free convection with the Zehnder–Mach interferometer, Wright–Patterson AFB Tech. Rep. No. 5747, ATI-44580 (1948).
22. T. J. Tritton, *Physical Fluid Dynamics*. Van Nostrand Reinhold, London (1979).
23. W. Hauf and U. Grigull, Optical methods in heat transfer, *Adv. Heat Transfer* **6**, 133–366 (1970).
24. W. J. King, The basic laws and data of heat transmission, *Mech. Engng* **54**, 347 (1932).

CONVECTION NATURELLE THERMIQUE LAMINAIRE AUTOUR DE BARRES HORIZONTALES A ARETES BRUSQUES AVEC ECOULEMENT DE SEPARATION

Résumé—La convection naturelle laminaire autour d'une barre horizontale à arêtes brusques, placée dans un fluide infini, a été étudiée numériquement et expérimentalement. Des solutions aux différences finies pour les équations bidimensionnelles de Navier–Stokes et de l'énergie sont obtenues pour deux configurations avec le nombre de Prandtl 0,7: une plaque plane d'épaisseur finie et une barre carrée. La difficulté associée au domaine complexe physique de l'écoulement est surmontée en utilisant des coordonnées adaptées. Dans l'étude numérique on ne trouve pas l'indication d'un écoulement avec séparation pour la plaque plane, dans le domaine de nombre de Rayleigh $10^3 \leqslant Ra \leqslant 10^5$. Pour la barre carrée, la couche limite se sépare aisément aux coins supérieurs pour $Ra \geqslant 5 \cdot 10^3$ et deux tourbillons jumeaux bien définis sont identifiés au dessus de la surface supérieure horizontale. Une étude interférométrique Mach–Zehnder est développée dans l'air pour déterminer les distributions de température et du nombre de Nusselt dans le domaine de nombre de Rayleigh $1{,}95 \cdot 10^4 \leqslant Ra \leqslant 1{,}53 \cdot 10^5$. La comparaison des résultats numériques et expérimentaux conduit à un bon accord.

WÄRMEÜBERGANG BEI LAMINARER NATÜRLICHER KONVEKTION AN SCHARFKANTIGEN WAAGERECHTEN STÄBEN MIT STRÖMUNGSABLÖSUNG

Zusammenfassung—Die laminare natürliche Konvektion an einem scharfkantigen waagerechten Stab im unendlichen Fluid wurde numerisch und experimentell untersucht. Lösungen der zweidimensionalen Navier–Stokes-Gleichungen wurden mit Hilfe finiter Differenzen für eine Prandtl-Zahl von 0,7 für den Fall einer ebenen Platte endlicher Dicke und für einen quadratischen Stab ermittelt. Probleme, die sich aus dem komplizierten Strömungsfeld ergaben, wurden durch dem Körper angepaßte Koordinaten gelöst. Aus der numerischen Untersuchung ergab sich für die waagerechte Platte kein Hinweis für eine Strömungsablösung, solange die Rayleigh-Zahl zwischen 10^3 und 10^5 liegt. Beim quadratischen Stab jedoch löste sich die Grenzschicht an den oberen scharfen Kanten bei $Ra \geqslant 5 \cdot 10^3$ ab, und es waren paarweise Wirbel oberhalb der waagerechten Oberfläche zu erkennen. Parallel dazu wurden Messungen mit einem Mach–Zehnder-Interferometer an einem quadratischen Stab in Luft durchgeführt, um die örtliche Verteilung von Temperatur und Nusselt-Zahl für Rayleigh-Zahlen zwischen $1{,}95 \cdot 10^4$ und $1{,}53 \cdot 10^5$ zu ermitteln. Der Vergleich zwischen experimentellen und theoretischen Ergebnissen ergab gute Übereinstimmung.

ЛАМИНАРНЫЙ ЕСТЕСТВЕННОКОНВЕКТИВНЫЙ ТЕПЛОПЕРЕНОС ОТ ГОРИЗОНТАЛЬНЫХ БРУСЬЕВ С ОСТРОЙ КРОМКОЙ В УСЛОВИЯХ ОТРЫВА ТЕЧЕНИЯ

Аннотация—Численно и экспериментально исследуется ламинарная естественная конвекция над горизонтальным бруском с острой кромкой, помещенным в неограниченный объем жидкости. Решение двумерных уравнений Навье–Стокса и энергии получены методом конечных разностей при заданном числе Прандтля 0,7 для двух конфигураций: плоская пластина конечной толщины и брусок квадратного сечения. Использование координат с началом в центре исследуемого тела устраняет трудности, связанные с физически сложными условиями течения. При численном исследовании не обнаружено отрыва течения для случая плоской пластины в диапазоне чисел Рэлея $10^3 \leq Ra \leq 10^5$. Однако в случае бруска квадратного сечения пограничный слой легко отрывается на верхних острых кромках при $Ra \geq 5 \cdot 10^3$ и над верхней горизонтальной поверхностью появляются четко выраженные двойные вихри. С помощью интерферометра Маха–Цендера проведены исследования на воздухе для бруска квадратного сечения, из которых найдены распределения локальных температуры и чисел Нуссельта в диапазоне чисел Рэлея $1{,}95 \cdot 10^4 \leq Ra \leq 1{,}53 \cdot 10^5$. Сравнение численных и экспериментальных результатов показало их хорошее согласие.